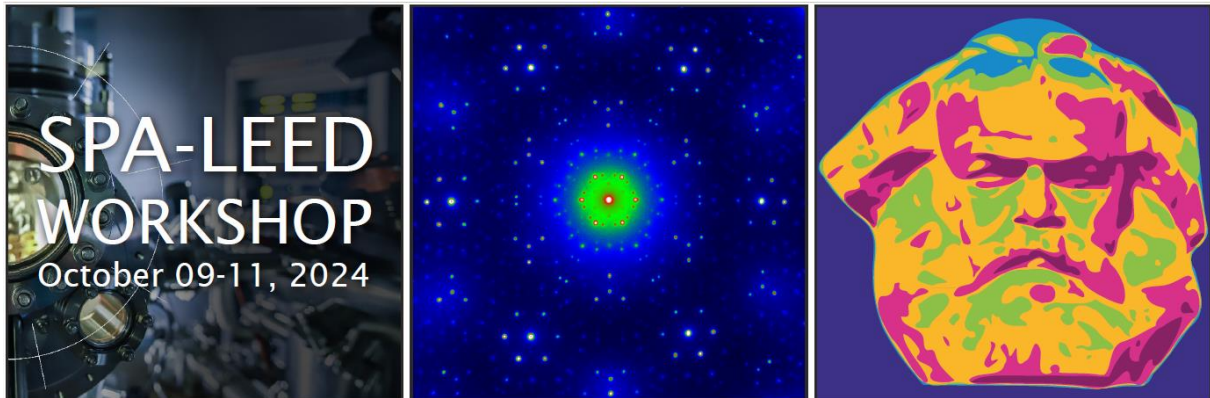


International workshop on SPA-LEED and related techniques



TECHNISCHE UNIVERSITÄT
CHEMNITZ



KULTURHAUPTSTADT
EUROPAS

Chemnitz, Germany

09-11 October 2024

Institute of Physics
Chemnitz University of Technology

The SPA-LEED workshop is supported by:

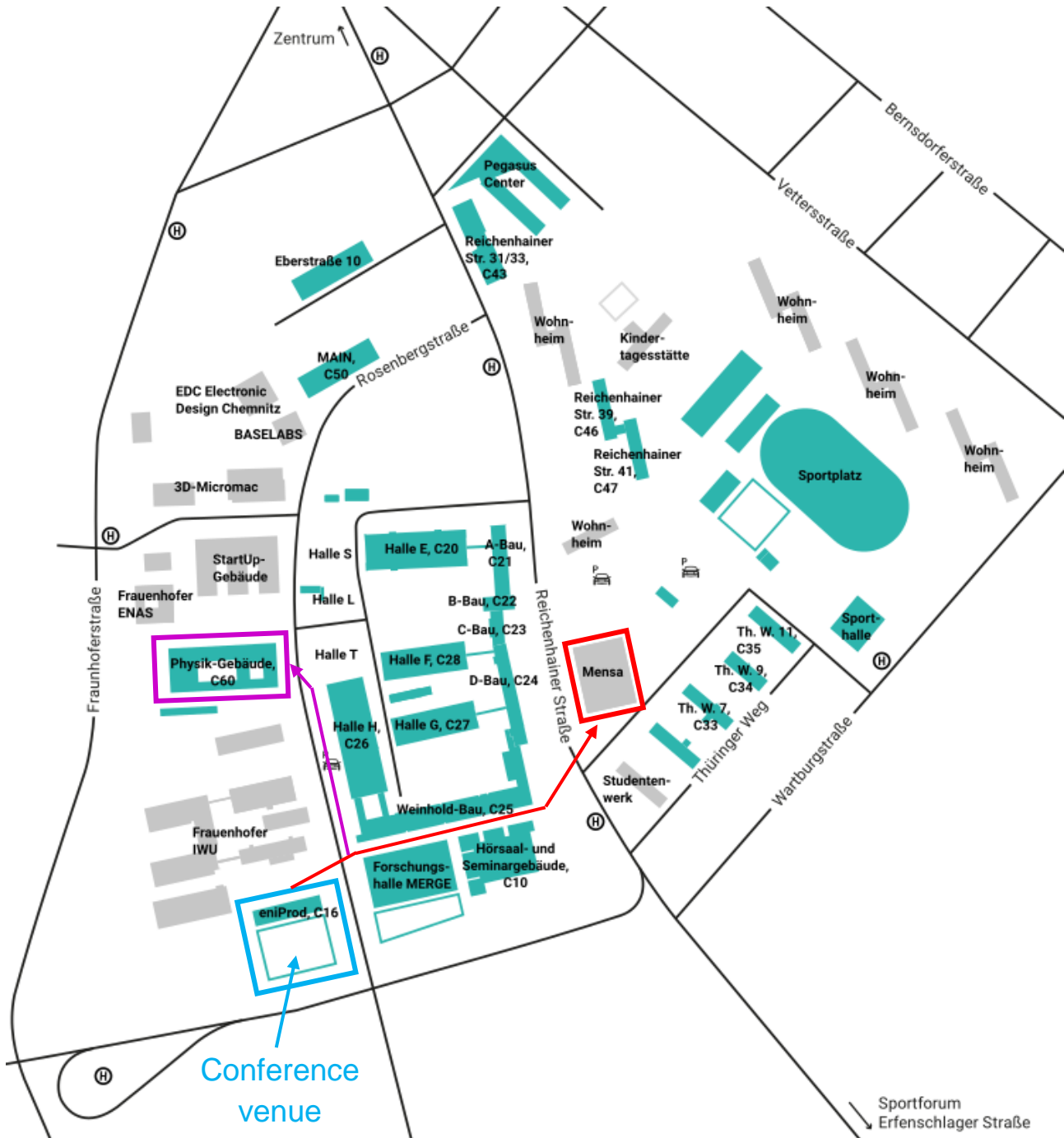


TECHNISCHE UNIVERSITÄT
IN DER KULTURHAUPTSTADT EUROPAS
CHEMNITZ


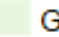





Map of the conference site:

(Conference room – Poster session – Labtours – Mensa)



<https://www.tu-chemnitz.de/tu/lageplan/campusfinder/campusfinder.html?id=2>

	Treppe		Gang		markiertes Objekt		Durchgang		Eingang
---	--------	---	------	---	-------------------	---	-----------	---	---------

Coffee breaks & Meals

- Lunch on Thursday 10 October is served in the Mensa, Reichenhainer Str. 55
- Lunch on Friday 11 October is served on the conference venue
- During the breaks coffee, tea, biscuits will be served next to the lecture hall
- During the poster session on Wednesday 9 October drinks are served
- Thursday evening: Buffet-style dinner (including meals for vegetarians) is served in the Restaurant Turm-Brauhaus, Neumarkt 2, 09111 Chemnitz. *(Please note that only non-alcoholic drinks are included)*

Internet access

eduroam and/or tuc-guest account *(please ask at the registration desk)*

Venue

TU Chemnitz, C16 eniPROD

Emergency and special help telephone

+49 371 53133103 (Christoph Tegenkamp)

Workshop Program

Wednesday (09.10.2024)

Time	Name	Title
15 ¹⁰ -15 ⁵⁵	Till Domröse invited	Nanobeam Ultrafast Electron Diffraction of Structural Phase Transformations
15 ⁵⁵ -16 ²⁰	Christian Brand	Ultrafast thermal boundary conductance under large temperature discontinuities of ultrathin epitaxial Pb films on Si(111)
16 ²⁰ -16 ⁴⁵	Herbert Pfnür	Concentration dependent (de-)stabilization of vicinal Si surfaces by adsorbed gold submonolayers
16 ⁴⁵ -18 ⁰⁰	Poster I	

Thursday (10.10.2024)

09 ⁰⁰ -09 ⁴⁵	Moritz Sokolowski invited	Layers of Large Organic Molecules - From SPA-LEED to IV-LEED and Reverse
09 ⁴⁵ -10 ¹⁰	Jens Falta	IV-LEEM and μ -LEED Study of the Oxidation of Alloyed Pt _{1-x} Sn _x /Pt(111)
10 ¹⁰ -10 ³⁵	Alexander M. Schneider	Structural analyses of Se and Te adsorbate phases on Ru(0001) using μ LEED-IV data
Conference photo		
Break		
11 ⁰⁵ -11 ⁵⁰	Michael Tringides invited	A long standing paradox: broad diffraction spots measure high quality 2D materials
11 ⁵⁰ -12 ¹⁵	Birk Finke	The Bell-Shaped Component in Diffraction from 2D Materials
12 ¹⁵ -12 ⁴⁰	Peter Kury	Latest developments regarding SPA-LEED software
Lunch		
14 ⁰⁰ -16 ⁰⁰	Poster II	
16 ⁰⁰ -17 ⁰⁰	Lab tours	
17 ⁰⁰ -17 ²⁵	Rico Ehrler	Advanced Modeling of X-ray Reflectivity for Thick Metallic Multilayer Systems
17 ²⁵ -17 ⁵⁰	Linus Pleines	In situ Study of the Identification of the Active Sites during Reoxidation of Ce ₂ O ₃ (111) on Ru(0001) by CO ₂
Dinner		

Friday (11.10.2024)

09 ⁰⁰ -09 ⁴⁵	Philip Schädlich invited	Low-energy Electron Microscopy: Stacking Relations and Graphene-Substrate Interactions
09 ⁴⁵ -10 ¹⁰	Stefan Förster	From simple to complex: A classification of quasicrystal approximants in two-dimensional Ba-Ti-O on Pd(111)
10 ¹⁰ -10 ³⁵	Marko Kriegel	Incommensurability and Negative Thermal Expansion of Single Layer Hexagonal Boron Nitride
Break I		
11 ⁰⁵ -11 ⁵⁰	Andreas Undisz invited	Spatially resolved phase detection in the near-surface area using TEM
11 ⁵⁰ -12 ¹⁵	Julian Koch	Proximitized Bi(110) quantum islands on epitaxial graphene
12 ¹⁵ -12 ⁴⁰	Lunch, Departure	

Poster Session

Poster N	Name	Title
P.1	Phiw-Ondee Satjawoot	Structural study of reactive growth and interaction between cerium oxide and graphene on Ru(0001)
P.2	Pavel Procházka	ProLEED Studio: Simplifying Modeling of Low-Energy Electron Diffraction Patterns
P.3	Chris Schröder	SPA-LEED studies of the ordering of Au-induced Nanowires on Si(553)
P.4	Joachim Wollschläger	SPA-LEED studies on the epitaxy of ultra-thin Fe ₃ O ₄ films on SrTiO ₃ (001)
P.5	Niels Ganser	UHV-CVD on Ir(111) for the Growth of 2D Materials
P.6	Mohammad Tajik	Order-disorder phase transition on the dimerized Si(001) surface
P.7	Christian Kumpf	Boron Nitride on SiC(0001): A pathway towards unconventionally oriented single-layer graphene and twisted bilayer graphene
P.8	Markus Gruschwitz	Imaging Charge Densities at Interfaces with TEM
P.9	Peter Richter	Growth of crystalline CoCrFeNi high-entropy alloy thin films on LaAlO ₃ by magnetron sputtering
P.10	Niclas Tilgner	Intercalation of Graphene on SiC: New Materials and Emerging Physics
P.11	Lukas Schewe	Composition and band structure of aluminum alloyed-gallium oxide by XPS
P.12	Sergii Sologub	Intercalation of Pb using buffer layer on SiC(0001)

Nanobeam Ultrafast Electron Diffraction of Structural Phase Transformations

Till Domröse^{1,2}, Thomas Danz¹, Leonardo da Camara Silva², Sophie F. Schaible^{1,2}, Kai Rossnagel^{3,4}, Sergey V. Yalunin¹, and Claus Ropers^{1,2}

¹Max Planck Institute for Multidisciplinary Sciences, Göttingen, Germany

²4th Physical Institute, Georg-August University Göttingen, Göttingen, Germany

³Institute of Experimental and Applied Physics, Kiel University, Kiel, Germany

⁴Ruprecht Haensel Laboratory, Deutsches Elektronen-Synchrotron DESY, Hamburg, Germany

Ultrafast transmission electron microscopy (UTEM) combines nanometer spatial with femtosecond temporal resolution (Fig. 1a), accessing non-equilibrium dynamics in heterogeneous systems [1,2]. Here, we study charge-density wave (CDW) phase transformations in the layered material 1T-TaS₂.

In ultrafast dark-field imaging, we trace the few-picosecond nucleation of an incommensurate (IC) phase after exciting the material's nearly-commensurate (NC) CDW with 5 nm spatial resolution [3]. In a complementary approach, a tomographic reconstruction of the diffraction spot shape in nanobeam ultrafast electron diffraction (Fig. 1c,d) elucidates the three-dimensional IC phase ordering [4]. In close analogy to a hexatic phase [5], we find that a network of unbound dislocations mediates the establishment of long-range order on ultrafast time scales via a light-induced hexatic state.

Methodologically, the structural transitions are driven at up to unprecedented megahertz repetition rates [6], and probed with highly coherent electron nanobeams [4]. Thus, our work will enable future UTEM measurements of functional materials and heterostructures with high resolution and sensitivity.

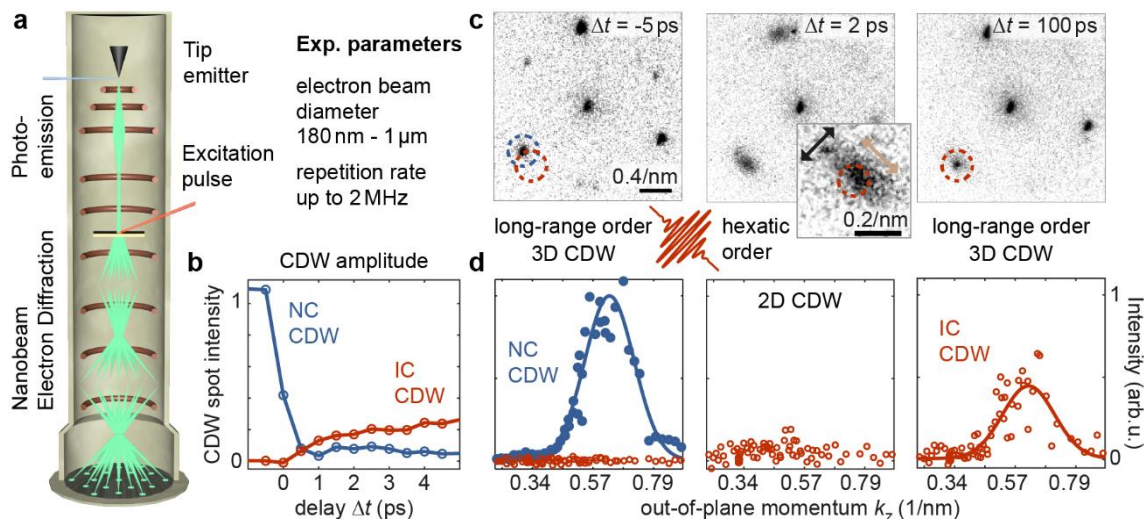


Figure 1 a) UTEM schematics. b) NC (blue) and IC (red) diffraction spot intensity after an optical excitation at $\Delta t=0$. c) In-plane dynamics. The transient hexatic is characterized by azimuthal spot broadening. d) Out-of-plane ordering. The CDW rocking curve indicates a dimensional cross-over.

- [1] A. Feist, *et al.*, *Ultramicroscopy* **176**, 63-73 (2017)
 [2] Th. Danz, T. Domröse, C. Ropers, *Science* **371(6527)**, 371-374 (2021)
 [3] T. Domröse, *et al.*, *Nature Materials* **22(11)**, 1345-1351 (2023)
 [4] D. Nelson, B. Halperin, *Physical Review B* **19**, 2457-2484 (1979)
 [5] T. Domröse, C. Ropers, arXiv:2402.02931 (2024)

Ultrafast thermal boundary conductance under large temperature discontinuities of ultrathin epitaxial Pb films on Si(111)

C. Brand¹, T. Witte¹, M. Tajik¹, J.D. Fortmann¹, B. Finke¹, M. Horn-von Hoegen^{1,2}

¹Faculty of Physics, University of Duisburg-Essen, Duisburg, Germany

²Center for Nanointegration Duisburg-Essen, Duisburg, Germany

The non-equilibrium dynamics of electrons in a metal subsequent to excitation with a fs-laser pulse couple to lattice degrees of freedom during the relaxation phase of the system. Here we have studied the lattice dynamics in ultrathin Pb films grown on Si(111) by means of ultrafast reflection high-energy electron diffraction. After thermalization of the electron and lattice system, the transient cooling of the film is determined by the heat transport across the interface into the substrate, i.e., by the thermal boundary conductance (TBC) on timescales of a few 100 ps [1]. For crystalline Pb films with low defect density at a base temperature of 19 K we experimentally find a TBC of less than 2 MW/m²K. We discuss the time-resolved results at different levels of the diffuse mismatch model.

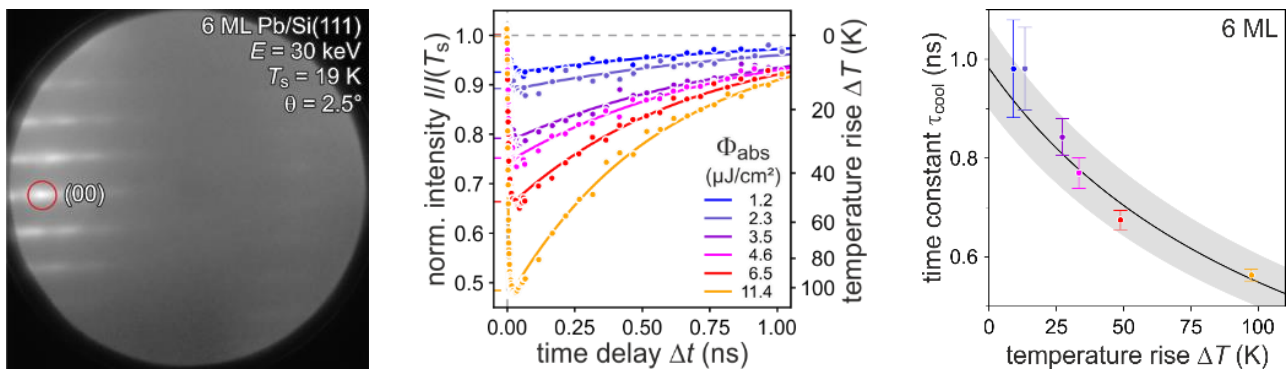


Figure 2: (left) Diffraction pattern of a 6 ML thin Pb film on Si(111) in RHEED. (center) Transient recovery of intensity during cooling for various absorbed laser fluencies. (right) Corresponding time constants.

[1] T. Witte et al., Appl. Phys. Lett., 110, 243103 (2017).

Concentration dependent (de-)stabilization of vicinal Si surfaces by adsorbed gold submonolayers

Zamin Mamiyev¹, Christoph Tegenkamp¹, Herbert Pfnür²

¹*Institut für Physik, Technische Universität Chemnitz, Reichenhainer Str. 70, D-09126 Chemnitz, Germany*

²*Institut für Festkörperphysik, Leibniz Universität Hannover, Appelstraße 2, D-30167 Hannover, Germany*

Stepped surfaces are always less stable compared to the flat reference system, ranging from metastability due to the macroscopic external miscut of a single crystal to high instability with phase separation into step bunches and low-index facets. This situation can be dramatically modified by the presence of adsorbate layers. Gold on Si surfaces is a well-known prominent example for adsorbate-induced faceting, even of flat surfaces [1]. Staying with Au on Si, we demonstrate here the opposite role of Au, i.e., there is also the possibility that gold submonolayers is able to stabilize a stepped surface. However, this situation turns into destabilization, once a certain critical gold concentration is exceeded.

We discuss here the examples of the vicinal Si(775) and Si(553) surfaces. On both surfaces, Au forms atomic double chains of Au at low Au concentrations. As shown by SPALEED analysis, the presence of Au improves and stabilizes the regular periodic Si step array as long as the Au concentration remains below optimal concentration for formation of one double chain per mini-terrace. Interestingly, higher Au concentrations first trigger the Si(775) surface to facet into a mixture of (775) and (553) orientations before both surface start to form (111) terraces with Au monolayer coverage and step bunches at the critical coverage of 0.52 ML of Au. The role of Au atoms located at step edges or within the wires are discussed.

In this context, and quite surprisingly, doping these wires by minor concentrations of additional Au, or by atomic H results in enforced stabilization of long-range order of the atomic Au double chains on Si(553) by interaction with the substrate, and, furthermore, in spontaneous self-healing of structural defects [2]. This is true even for random adsorbate distribution. Combining atomistic models within density functional theory with low energy electron diffraction and high-resolution electron energy loss spectroscopy, we demonstrate that this apparently counterintuitive behavior is mainly caused by adsorption-induced band filling of modified surface bands, i.e., by the strong electronic correlation throughout the whole terrace. Although adsorption preferably occurs at the step edge, it enhances the dimerization and the stiffness of the Au dimers. Thus, the intertwinement of quasi-1D properties with delocalized 2D effects enforces the atomic wire order.

[1] H. Minoda, K. Yagi, F. Meyer zu Heringdorf, A. Meier, D. Kähler, M. Horn-von Hoegen, Phys. Rev. B. 59, 2363 – 2375 (1999).

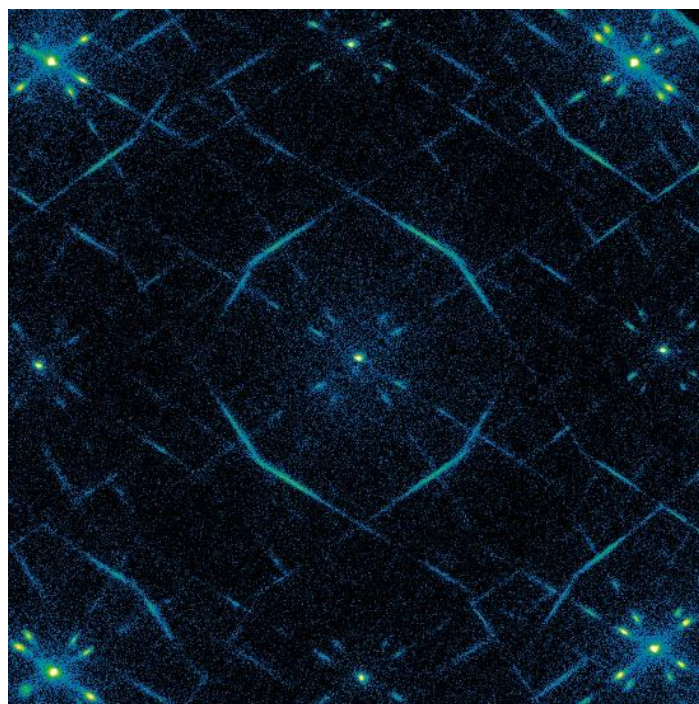
[2] Z. Mamiyev, C. Fink, K. Holtgrewe, H. Pfnür, S. Sanna, Phys. Rev. Lett. 126, 106101 (2021)

Layers of Large Organic Molecules - From SPA-LEED to IV-LEED and Reverse

Moritz Sokolowski¹

¹*Clausius-Institut für Physikalische und Theoretische Chemie
Rheinische Friedrich-Wilhelms-Universität*

Ordered monolayers of large organic molecules provide an ample playground for the application of LEED and in particular SPA-LEED for different reasons. First of all, the high resolution of SPA-LEED in k-space supports the analysis of the organic superstructures with their large unit cells. This includes the determination of their epitaxial relations with substrate surfaces. Secondly, profiles of organic layers bear information about the specific temperature and coverage dependent structural defects that are present in molecular structures due to the specific intermolecular interactions. Finally, it turns out that the limited-space resolution of conventional LEED optics limits the accessible k-space when large superstructures of organic molecules are measured for LEED-IV analysis. This motivates to develop the SPA-LEED instrumentation further in order to make it suitable for recording of LEED-IV curves. In this talk I will report on these topics using examples from different systems we have investigated over last years.



SPA-LEED image of the α phase of quinacridone on Ag(100). The prominent stripes are related to the lack of coherence between the individual linear and one-dimensional QA chains. Recorded by Morris Mühlpointner,. For a reference see also [1].

[1] N. Humberg, R. Bretel, A. Eslam, E. Le Moal, and M. Sokolowski, *J. Phys. Chem. C*, 24861-24873, 124 (2020).

Alloyed $\text{Pt}_{1-x}\text{Sn}_x/\text{Pt}(111)$ and Exposure to Molecular and Atomic Oxygen

Jens Falta¹

¹*Institute of Solid State Physics, University of Bremen, Germany*

Using IV-LEEM and μLEED , we have studied the oxidation of alloyed tin-poor $\text{Pt}_{1-x}\text{Sn}_x/\text{Pt}(111)$ surfaces in dependence of substrate temperature, oxygen dose, and upon exposure to both, molecular and atomic oxygen. Well-ordered surfaces were prepared by MBE evaporation of Sn on Pt(111) at high temperatures. This approach allows for a precise control over the amount of tin available for subsequent oxide formation and reduces the complexity of the platinum-tin model system by excluding Sn segregation from the bulk as a source for additional surface tin. Depending on the Sn deposit, we find the formation of $\text{Pt}_2\text{Sn}/\text{Pt}(111)$ and $\text{Pt}_3\text{Sn}/\text{Pt}(111)$ surface layers, respectively. The (2×2) reconstruction, indicative of $\text{Pt}_3\text{Sn}/\text{Pt}(111)$, initially appears, and shows its' maximum LEED intensity at 0.25 ML. The $(\sqrt{3}\times\sqrt{3})R30^\circ$ reconstruction is related to Pt_2Sn and evolves in coexistence with the (2×2) . With increasing deposits, solely the $(\sqrt{3}\times\sqrt{3})$ phase is found. Oxidation with molecular oxygen lead to strikingly distinct results for these two surfaces. For exposure of the tin poor $\text{Pt}_3\text{Sn}/\text{Pt}(111)$ no sign of oxidation was found even for large doses of O_2 . For the tin-richer surface of $\text{Pt}_2\text{Sn}/\text{Pt}(111)$, however, the evolution of an incommensurate rectangular structure is seen. This phase has also been found upon oxidation of $\text{Pt}_3\text{Sn}(111)$ in coexistence with other phases [1] and its' structure is very similar to that of other (111) oxides such as $z\text{-TiO}_x/\text{Pt}(111)$, $z\text{-TiO}_x/\text{Pd}(111)/\text{TiO}_2$, $z\text{-TiO}_x/\text{Pt}_3\text{Ti}(111)$, and $z\text{-VO}_x/\text{Pd}(111)$ and to that reported but not further investigated by Batzill et al. [2] after oxidation with NO_2 . Exposure to atomic oxygen lead to the formation of three different tin oxide phases. Initially, two new phases formed in coexistence: a metallic tin-poor (2×2) phase and an oxide phase, very similar to Structure I (Batzill). With increasing exposure, the (2×2) disappears and the rectangular structure (see above) is formed, first coexisting with Structure I before this vanishes and the rectangular structure remains and serves as template for subsequent reactive SnO_x growth.

[1] L. Merte, et al., J. Phys. Chem. C, 127 (2023)

[2] M. Batzill et al., Phys. Rev. B 69 (2004)

Structural analyses of Se and Te adsorbate phases on Ru(0001) using μ LEED-IV data

M. Alexander Schneider¹, Lars Buß², Anna Jana Ohlendorf³, Thomas Schmidt³, Jens Falta³, Jan Ingo Flege²

¹*Solid State Physics, Friedrich-Alexander-U. Erlangen-Nürnberg (FAU), Erlangen, Germany*

²*Appl. Physics and Semiconductor Spectroscopy, BTU Cottbus-Senftenberg, Cottbus, Germany*

³*Institute of Solid State Physics, University of Bremen, Bremen, Germany*

The identification of adsorption sites of single atoms is one of the most prominent issues where structure analyses by surface sensitive diffraction methods are needed [1]. We investigate here Se and Te adsorbed on the clean Ru(0001) surface. Similar to S on Ru(0001) [2], with increasing coverage a sequence of ordered structures is observed: (2×2) -X, $(\sqrt{3}\times\sqrt{3})R30$ -X, and the $c(2\times 4)$ -2X (X=Se,Te). Applying the recently developed ViPERLEED package [3] to μ LEED-IV data acquired using LEEM we show that high quality structural analyses with Pendry R-factors well below 0.2 can be obtained allowing for a definite characterization of the adsorption site and substrate relaxations.

We compare the findings to comparable structures found for Te on Ir(111) [1] also in view of the obtained accuracy of the analyses. Since LEEM would in principle allow to single out single structural domains on the surface [4], we discuss the requirements and limitations for more complex structural analyses of surfaces using μ LEED-IV.

[1] L. Hammer, A. Schewski, A. Wegerich, T. Kießlinger, M.A. Schneider, *Surface Science*, 122589, 750 (2024).

[2] R. Dennert, M. Sokolowski, H. Pfnür, *Surface Science*, 1, 271 (1992)

[3] F. Kraushofer, et al, arXiv:2406.18821 (2024) and M. Schmid et al., arXiv:2406.18413 (2024)

[4] J. de la Figuera, M. Puerta, J.I. Cerda, F. El Gabaly, K.F. McCarty, *Surface Science*, L105, 600 (2006)

A long-standing paradox: broad diffraction spots measure high quality 2D-materials

M.C.Tringides

Ames National Laboratory, Ames, Iowa 50011, USA

Department of Physics and Astronomy, Iowa State University, Ames, Iowa 50011, USA

Paradoxically a very broad diffraction background, named the Bell-Shaped-Component (BSC), has been established as a feature of graphene growth. Recent diffraction studies as a function of electron energy on Gr/SiC have shown that the BSC is not related to scattering interference. The broad background is in-phase with the Bragg component of both the (00) and Gr(10) spots [1]. Instead textbook diffraction states it should be out-of-phase, since it should originate from destructive interference between adjacent terraces. Additional experiments were carried out as a function of temperature over the range 1200 °C-1300 °C that single-layer-graphene (SLG) grows. Quantitative fitting of the profiles shows that the BSC follows the increase of the G(10) spot, proving directly that the BSC indicates high quality graphene [2]. The BSC has been also in graphene on metals including Gr/Ir(111) [3]. Recent experiments also show that the BSC is present in h-BN films grown on Ir(111) [3,4]. Its presence in such a wide range of 2-materials suggests its origin must be general and fundamental related to the unusual single layer uniformity common to these widely varying films. One possible explanation of the BSC relates to electron confinement within a single uniform layer which suggests that the BSC is an excellent measure of their uniformity. The confinement of the graphene electrons and the corresponding spread in their wavevector has been seen with ARPES [5]. The transfer of the large momentum spread to the diffracted electrons requires better theoretical understanding of the graphene electron-beam electron interaction.

In collaboration with S. Chen, P.A.Thiel (deceased), M. Horn von Hoegen, S. Chen, E. H. Conrad., M.Petrovic, F-J. Meyer zu Heringdorf

[1] S. Chen, et al. Phys. Rev. B. 100, 155307 (2019).

[2] S. Chen, et al. J. Phys. Chem. Lett. 11, 8937 (2020).

[3] K. Omambac et al , Appl. Phys. Lett. 118, 241902 (2021)

[4] M. Petrovic et al Nanotechnology 32 505706 (2021)

[5] T. Ohta et al. Phys. Rev. Lett. 98, 206802 (2007).

The Bell-Shaped Component in Diffraction from 2D Materials

Birk Finke¹, Christian Brand¹, Karim Omambac¹, Pascal Dreher¹, Hannah Kohler¹,
Frank-J. Meyer zu Heringdorf¹⁻³, Michael Horn-von Hoegen^{1,2}

¹*Faculty of Physics, University of Duisburg-Essen, Duisburg, Germany*

²*Center for Nanointegration Duisburg-Essen, Duisburg, Germany*

³*Interdisciplinary Center for Analytics on the Nanoscale, Duisburg Germany*

In 2D materials, the formation of moiré superlattices with graphene or hBN on crystalline surfaces alters electronic, vibrational, and chemical properties. Here we analysed an unusual broad diffraction background observed in low energy electron diffraction from 2D material systems as is shown in Fig. 1 which is called the bell-shaped component (BSC) [1-3]. Employing SPA-LEED, LEEM, and μ -LEED we propose the origin to be the inelastic scattering of the low energy electrons at the vertically polarized ZA-phonons of the weakly bound graphene and hBN layers on Ir(111) and SiC(0001). For these systems the ZA-phonon branch exhibits a parabolic dispersion with a finite phonon frequency of a few meV at the Γ point. This results in a high phonon density at low energy but high momentum causing the strong intensity of the BSC in diffraction. In the framework of kinematic scattering theory, we performed simulations of the inelastic diffuse scattering which quantitatively confirm our proposal.

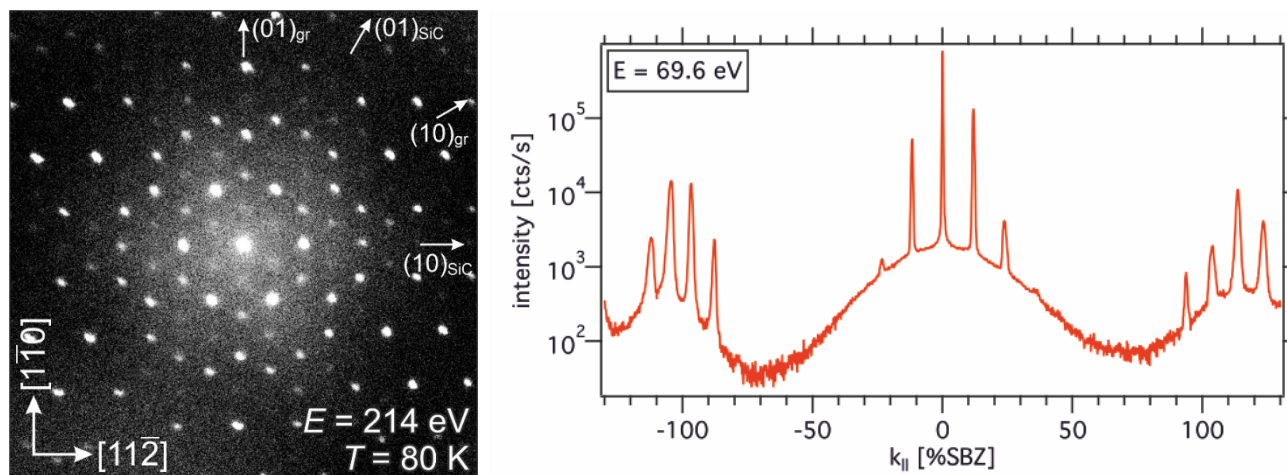


Figure 1: (left) SPA-LEED pattern of epitaxial monolayer graphene on 4H-SiC(0001). The broad circular-shaped inelastic “diffuse” intensity centered at the (00) spot is the bell-shaped component. (right) Linescan of graphene on Ir(111) at 300 K where the BSC is dominant in diffraction.

[1] S. Chen et al., Phys. Rev. B **100**, 155307 (2019)

[2] M. Petrović et al., Nanotechnology **32**, 505706 (2021)

[3] K. Omambac, B. Finke et al., Appl. Phys. Lett. **118**, 241902 (2021)

Latest developments regarding SPA-LEED software

Peter Kury, Dirk Hänsel¹

¹*out-of-the-box systems GmbH, Breddebuschhang 5c, 45257 Essen*

The most recent new features of the SPA-LEED software WinSPA are presented in detail:

Being a scanning data acquisition method, one of the few fundamental disadvantages of SPA-LEED is the low speed of data acquisition. A big improvement can be realized by varying the counter gate time depending on the detected count rate, spending less measurement time at low intensity regions of the diffraction image [1]. This enables to acquire even 3D reciprocal space maps in a reasonable amount of time.

Another typical problem of all LEED methods are image distortions [2]. WinSPA now contains the option for software correction of low order radial distortions as well as an advanced 1D scan with precisely centered diffraction spots on the scan path.

While reciprocal space maps (RSM) were possible with SPA-LEED for more than 20 years [3], a recent improvement allows to take I(V) curves via SPA-LEED. In order to achieve good focus properties on a large range of electron energies, a full software control of the electron gun lens system was implemented.

Additionally, a correction of nonlinearities of the channel electron multiplier, partially by hardware improvements, but also via a software option was added to WinSPA [4]. Some additional features such as the macro commander, the exclusion zone and the advanced scan capability by superposition of real space and reciprocal space scanning will also be discussed.

[1] Anna J. Kny, Moritz Sokolowski, Peter Kury "Increasing the scan speed in high resolution, low energy electron diffraction measurements by presetting the gate time" Rev. Sci. Instrum. 94, 064707 (2023), <https://doi.org/10.1063/5.0137991>

[2] Falko Sojka, Matthias Meissner, Christian Zwick, Roman Forker, Torsten Fritz "Determination and correction of distortions and systematic errors in low-energy electron diffraction" Rev. Sci. Instrum. 84, 015111 (2013), <https://doi.org/10.1063/1.4774110>

[3] F.-J. Meyer zu Heringdorf, M. Horn-von Hoegen "Reciprocal space mapping by spot profile analyzing low energy electron diffraction" Rev. Sci. Instrum. 76(8):085102/1-5 (2005), <http://dx.doi.org/10.1063/1.1988287>

[4] M.P. Seah "Channel electron multipliers: quantitative intensity measurement—efficiency, gain, linearity and bias effects" J. El. Sp. Rel. Ph. 50(1), 137-157 (1990), [https://doi.org/10.1016/0368-2048\(90\)80015-3](https://doi.org/10.1016/0368-2048(90)80015-3)

Advanced Modeling of X-ray Reflectivity for Thick Metallic Multilayer Systems

Rico Ehrler^{1,2}

¹*Chemnitz University of Technology, D-09107 Chemnitz, Germany*

²*Research Center MAIN, D-09126 Chemnitz, Germany*

X-ray reflectivity (XRR) is a versatile, nondestructive technique for probing thin film systems at grazing incidence, offering insights into layer thickness, roughness, and density. It specifically probes the scattering length density (SLD), representing the lateral average electron density as a function of sample depth. However, due to the inherent phase problem in X-ray techniques, where phase information is lost during the measurement, extracting the SLD from XRR data requires careful sample modeling. As the complexity of the sample increases, so does the complexity of the required models. Additionally, microstructure effects have to be considered, as XRR averages laterally over the sample, in contrast to localized techniques like transmission electron microscopy (TEM).

In this talk, I will explore the application of XRR to the structural characterization of thick metallic Co/Pt ML systems, where attribution of features within the XRR signal can be challenging. I will discuss different modeling approaches using the open-source software 'GenX 3' [1], including a simplified model that can provide substantial insights, even without incorporating the actual quite complex ML structure. Furthermore, a more detailed model of the full sample will also be presented, developed using the simplified model as well as TEM images to create a 1D representation of the 3D microstructure.

[1] A. Glavic and M. Björck, J. Appl. Cryst., p1063-1071, vol. 55 (2022)

In situ Study of the Identification of the Active Sites during Reoxidation of Ce₂O₃(111) on Ru(0001) by CO₂

L. Pleines¹, L. Buß², T. O. Menteş³, A. Locatelli³, J. Falta^{1,4}, J. I. Flege²

¹*Institute of Solid State Physics, University of Bremen, Bremen, Germany*

²*Applied Physics and Semiconductor Spectroscopy, Brandenburg University of Technology Cottbus-Senftenberg, Cottbus, Germany*

³*Elettra-Sincrotrone Trieste S.C.p.A., Trieste, Italy* ⁴*MAPEX Center for Materials and Processes, University of Bremen, Bremen, Germany*

Cerium oxide is of great technological interest due to its relevance in various catalytic applications. An inverse model catalyst such as cerium oxide on Ru(0001) can be used to understand the fundamentals behind catalytic processes. For the production of methanol from CO₂ and H₂, oxygen vacancies, as found on reduced ceria, are necessary to activate the CO₂ molecules. We have grown CeO₂(111) islands on Ru(0001), identified by μ LEED and I(V)-LEEM. Afterwards, we reduced the ceria islands following recipes of previous work by exposure to H₂ [1] and by thermal treatment [2]. Finally, we studied the interaction of CO₂ with islands of reduced ceria in situ by a combination of dynamic (real-time) I(V)-LEEM and spatially resolved x-ray absorption spectroscopy (XAS-PEEM) at the ELETTRA nanospectroscopy beamline. In particular, the oxidation state was derived from specific islands by fitting the data by a linear combination of reference spectra of Ce₂O₃ (Ce³⁺) and CeO₂ (Ce⁴⁺). Partial reoxidation by exposure to CO₂ was investigated at 540 °C. From the analysis we derive a correlation of the oxidation state and the size of the island, revealing that larger islands are more oxidized throughout this process (Figure 1). We attribute this finding to a larger thickness of these islands [3]. Furthermore, the different electron escape depths of I(V)-LEEM and XAS-PEEM allow comparing the oxidation state of the topmost layers and the bulk. Fitting the I(V)-LEEM data was used to derive a pixel resolved map of the oxidation state providing further insight into the distribution of active sites of the cerium oxide islands on the nanometer scale.

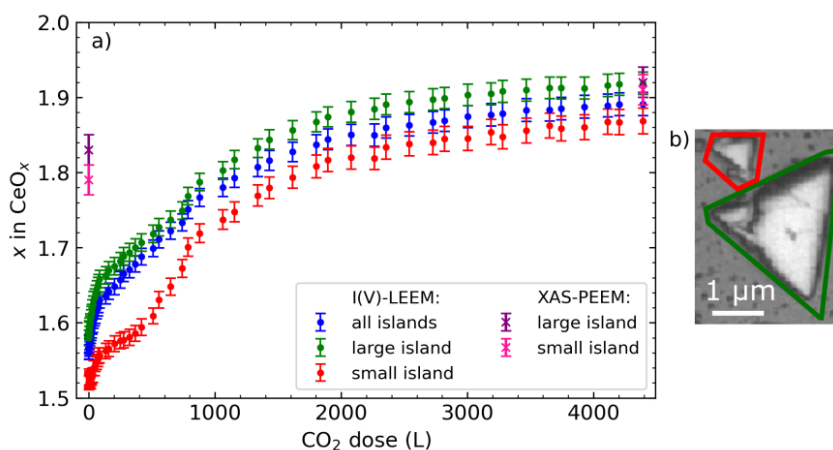


Figure 1: a) Oxidation states of different CeO_x islands during exposure to CO₂. b) Image of the small (red) and large (green) island.

[1] J. Höcker, T. O. Menteş, A. Sala, A. Locatelli, T. Schmidt, J. Falta, S. D. Senanayake, J. I. Flege, *Adv. Mat. Interfaces* 1500314, 2 (2015)

[2] J. Höcker, J. O. Krisponeit, T. Schmidt, J. Falta, J. I. Flege, *Nanoscale* 9352, 9 (2017)

[3] A. Schaefer, B. Hagman, J. Höcker, U. Hejral, J. I. Flege, J. Gustafson, *Phys. Chem. Chem. Phys.*, 19447, 20 (2018)

Low-energy Electron Microscopy: Stacking Relations and Graphene-Substrate Interactions

Philip Schädlich^{1,2}, Thomas Seyller^{1,2}

¹*Chemnitz University of Technology, Institute of Physics, Reichenhainer Straße 70, 09126 Chemnitz, Germany*

²*Center for Materials, Architectures and Integration of Nanomembranes (MAIN), Rosenbergstraße 09126 Chemnitz, Germany*

In this contribution, we present a two-part study focusing on the properties of graphene on different substrates, utilizing advanced electron diffraction and microscopy techniques based on low-energy electron microscopy (LEEM).

In the first part, we investigate graphene grown on silicon carbide (SiC) substrates with varying surface terminations, which are accessible only via the polymer-assisted sublimation growth (PASG). Using bright-field and dark-field microscopy, we successfully identify the distinct terminations and observe a nuanced dependence of the graphene properties on the specific substrate termination [1,2]. These findings provide critical insights into the role of substrate interactions in tailoring the electronic properties of graphene.

The second part of our study explores chemical vapor deposition (CVD)-grown graphene on copper foil. We examine the relationship between the faceting of the copper substrate and the stacking domains of graphene. Remarkably, we demonstrate that these stacking domains persist even after the graphene is transferred onto a secondary target substrate [3]. This persistence highlights the robustness of the stacking domains and the potential implications for stacking engineering in 2D heterostructures.

[1] D.M. Pakdehi, P. Schädlich, T.T.N. Nguyen, A.A. Zahkharov, S. Wundrack, E. Najafidehaghani, F. Speck, K. Pierz, Th. Seyller, C. Tegenkamp, H.W. Schumacher, *Adv. Funct. Mater.* 2004695, 30 (2020).

[2] A. Sinterhauf, G.A. Traeger, D.M. Pakdehi, P. Schädlich, P. Willke, F. Speck, Th. Seyller, C. Tegenkamp, K. Pierz, H.W. Schumacher, M. Wenderoth, *Nature Communications* 555, 11 (2020).

[3] P. Schädlich, F. Speck, C. Bouhafs, N. Mishra, S. Forti, C. Coletti, Th. Seyller, *Adv. Mater. Interfaces* 2002025, 8 (2021).

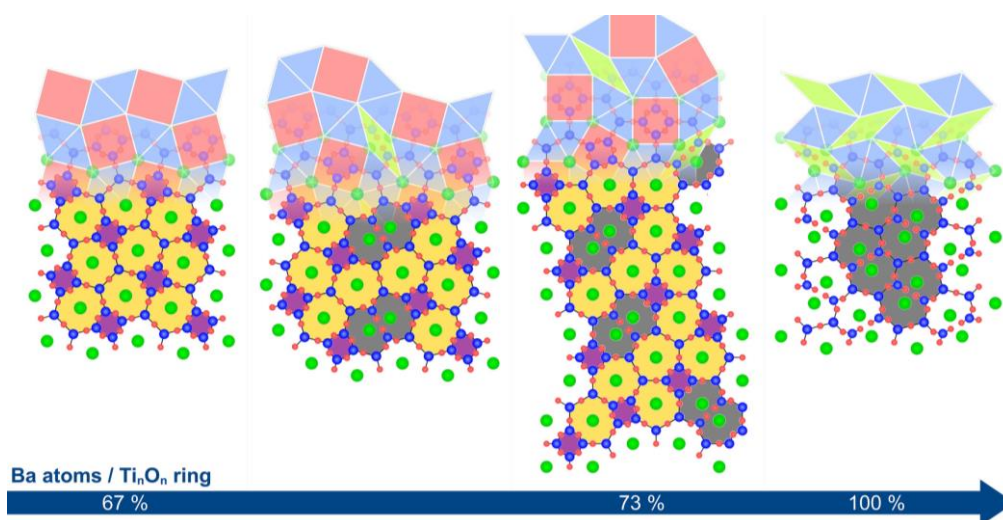
From simple to complex: A classification of quasicrystal approximants in two-dimensional Ba-Ti-O on Pd(111)

Stefan Förster, Friederike Wühlrl, Sebastian Schenk, and Wolf Widdra

Institute of Physics, Martin-Luther-Universität Halle-Wittenberg, Halle, Germany

Dodecagonal quasicrystals in two-dimensional ternary oxides have been discovered a decade ago [1]. With the recent experimental validation of the structure model by Cockayne et al., a new level of understanding for this class of aperiodic materials is reached [2]. On the atomic level, all oxide quasicrystals known so far consist of Ti_nO_n rings with ring sizes $n = 4, 7, 10$ with alkaline earth metal ions decorating the 7 and 10 membered rings. In total, 73% of all rings are occupied in this dodecagonal network structure. The alkaline earth metal atoms form the vertices of a square-triangle-rhombus tiling. The detailed knowledge about the atomic structure allows to classify the wealth of quasicrystal-related periodic approximant structures by their alkaline earth metal ion concentration.

Here we present the series of approximant structures observed in Ba-Ti-O on Pd(111) [3,4]. These periodic structures range from simple square-triangle and square-rhombus tilings with four alkaline earth metal ions per unit cell to complex square-triangle-rhombus tilings with 60 alkaline earth metal ions per repeating unit. In this contribution we demonstrate how these structures evolve from one another as a consequence of packing density optimization. The evolution of structural complexity is also followed from a diffraction point of view.



Phase diagram of different long-range ordered structures for Ba-Ti-O on Pd(111) depending on their relative Ti_nO_n ring occupation with Ba ions

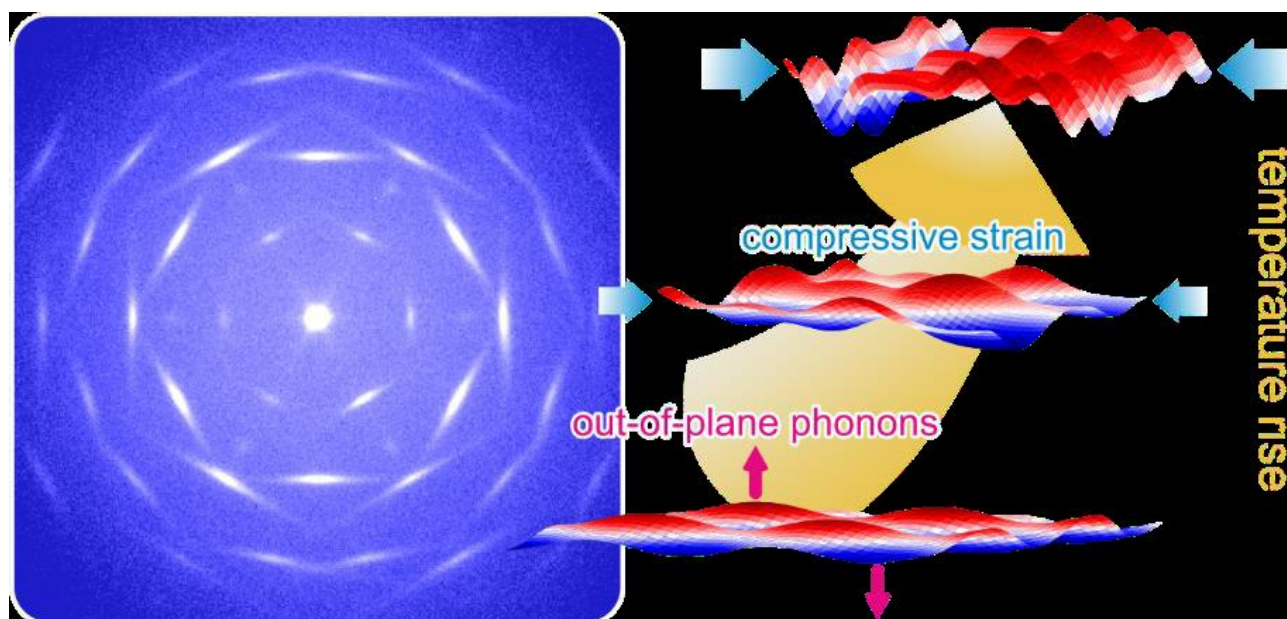
- [1] S. Förster, R. Hammer, M. Trautmann, K. Meinel & W. Widdra, *Nature* 215, 502 (2013)
- [2] S. Schenk et al., *Nat. Commun.* 7542, 13 (2022)
- [3] F. E. Wühlrl, O. Krahn, S. Schenk, S. Förster & W. Widdra, *PSS B* 2100389, 259 (2022)
- [4] F. E. Wühlrl, O. Krahn, S. Schenk, W. Widdra & S. Förster, *Phys. Rev. B* 195414, 107 (2023)

Incommensurability and Negative Thermal Expansion of Single Layer Hexagonal Boron Nitride

Marko A. Kriegel¹, Karim M. Omambac¹, Steffen Franzka², Frank-J. Meyer zu Heringdorf^{1,2}, Michael Horn-von Hoegen¹

¹Faculty of Physics and Center for Nanointegration Duisburg-Essen (CENIDE), University Duisburg-Essen, Lotharstr. 1, 47057 Duisburg, Germany

²Interdisciplinary Center for Analytics on the Nanoscale (ICAN), Carl-Benz-Str. 199, 47057 Duisburg, Germany



The emerging field of straintronics, i.e., the control and utilization of the strain state of a 2D material, is of great importance for their technological development, specifically in view of their future incorporation into van der Waals heterostructures. To gain fundamental insights into structural peculiarities of two-dimensional systems, single layer hexagonal boron nitride (*h*BN) grown on Ir(111) by chemical vapor deposition was used as a prototypical model system: High-resolution reciprocal space mapping by SPA-LEED reveals the incommensurate nature of the material system by measuring the *h*BN in plane lattice parameter with high precision, facilitated by the moiré magnification effect in diffraction. In a growth temperature (*T*_g) regime of 700-1150 °C an average lattice parameter of $2.496 \pm 0.006 \text{ \AA}$ was found. Eventually, careful disentanglement of the *h*BN's and substrate's behavior for rising *T*_g allowed the determination of a negative thermal expansion coefficient of $\alpha_{hBN} = -2.4 \times 1.2 \pm 10^{-6} \text{ K}^{-1}$. [1]

[1] M. A. Kriegel, K. M. Omambac, S. Franzka, F.-J. Meyer zu Heringdorf, M. Horn-von Hoegen, *Appl. Surf. Sci.* **624** (2023) 157156

Spatially resolved phase detection in the near-surface area using TEM

Andreas Undisz

*Chemnitz University of Technology, Institute of Materials Science and Engineering,
Erfenschlager Str. 73, 09125 Chemnitz*

Manufacturing and application of modern technical materials are often linked to thermo-mechanical treatments and subsequent use in aggressive environments, e.g., at elevated temperatures or in corrosive media. Intentional or unintentional, this causes changes to the microstructure that alter the material properties and thus the material behavior in the short and long term. Due to various aspects, material changes often occur initially in the vicinity of interfaces, especially near the material surface. Analytical access, already at these early stages, is important in order to identify fundamental processes and to design strategies for optimizing materials properties. Access with atomic resolution is made possible, for example, by transmission electron microscopy (TEM), requiring careful preparation of samples without introducing artifacts.

In this paper, examples of alloys are presented, and it is shown how the formation and transformation of phases near the surface can be identified and monitored at early stages by means of surface-preserving targeted preparation and TEM. The first example is a Ni-Ti alloys that is known to combine pseudoelastic behavior and biocompatibility, rendering it a successful material for minimally invasive implants [1]. During the processing of thin NiTi wires or tubes to medical implants, annealing for seconds to minutes at elevated temperature is required. In the specific case, this leads to the formation of an oxide layer that is only a few nanometers thin, but rich in Ti. Consequently, the Ni/Ti ratio in the alloy below the oxide shifts to Ni-rich, increasing the local thermodynamic driving force for phase transformations. It is observed that the formation of Ni-rich phases occurs unexpectedly fast, omitting the usually necessary timespan span required for incubation of crystalline phases in classical phase formations [2]. Already at the length scale of less than 20nm and for annealing durations as short as 120s, local phase transformation toward a metastable Ni₄Ti₃ phase is observed. With time, the transformation proceeds towards Ni₃Ti. Furthermore, examples of Cr-containing alloys and complex concentrated alloys/ high entropy alloys (CCA/ HEA) are presented with a focus on the formation of oxide phases at the surface during the early stages of oxidation, including discussion of implications of identified phases for the behavior of the alloys on the short and longer term [3,4].

[1] S. Nagaraja, R. Brown, D. Saylor, A. Undisz, *Shape Memory and Superelasticity*, 45–63, 8 (2022).

[2] K.E. Freiberg, R. Wonneberger, M. Seyring, M. Rettenmayr, A. Undisz, *Intermetallics*, 107817, 154 (2023).

[3] J. Apell, R. Wonneberger, H. Stöcker, P. Meye, K.E. Freiberg, M. Seyring, S. Lippmann, A. Undisz, *Corrosion Science*, 111594, 225 (2023).

[4] J. Apell, R. Wonneberger, M. Seyring, H. Stöcker, M. Rettenmayr, A. Undisz, *Corrosion Science*, 109642, 190 (2021).

Proximitized Bi(110) quantum islands on epitaxial graphene

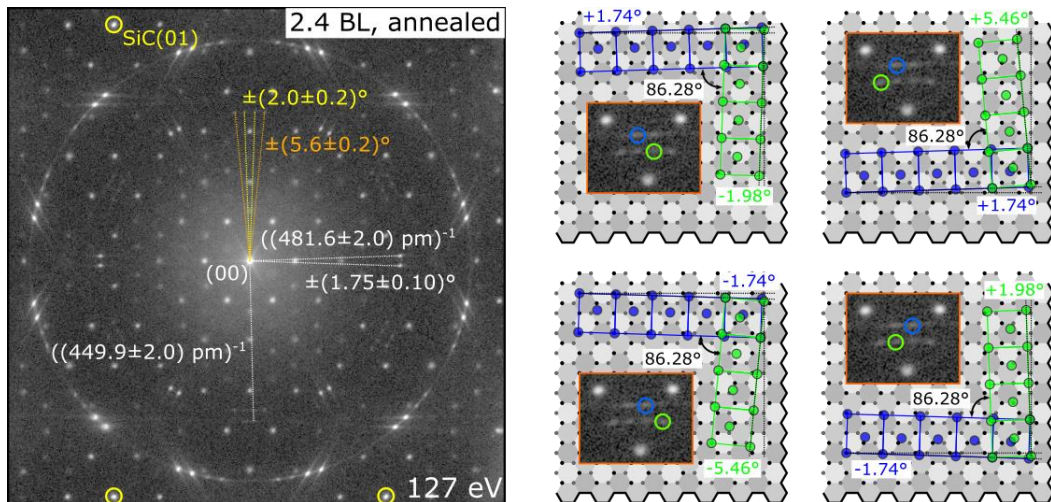
Julian Koch¹, Chitran Ghosal¹, Sergii Sologub^{1,2}, and Christoph Tegenkamp¹

¹*Institut für Physik, Technische Universität Chemnitz, Reichenhainerstr. 70, 09126 Chemnitz, Germany*

²*Institute of Physics, National Academy of Sciences of Ukraine, Nauki avenue 46, 03028 Kyiv, Ukraine*

The proximity effect allows for the functionalization of graphene by introducing properties into it that are not inherent to it. In this study, epitaxial Bi(110) islands were deposited on monolayer graphene (MLG)/SiC(0001) with the aim of increasing graphene's negligible spin-orbit interaction, and investigated by electron diffraction, scanning tunneling microscopy and magnetotransport.

The deposition at 300 K resulted in the formation of a majority of needle-like Bi(110) islands elongated in the Bi(110) zig-zag direction, which are aligned with the MLG armchair direction except for a small misalignment angle of about 1.75°. Additionally, we observed a minority of needle-like Bi(110) islands orientated roughly orthogonal to the majority structure, whose concentration significantly increased after an annealing step at 410 K. This minority structure has four sub-domains, which we attribute to the formation of mirror twin boundaries, resulting in two potential alignments of Bi(110) majority and minority domains with respect to each other, in addition to two possible alignments of the majority domain with respect to graphene (see figure).



LEED image for a Bi coverage of 2.4 BL after annealing at 410 K for 30 min recorded at 127 eV (left). Alignment of the Bi(110) majority (blue) and minority (green) islands with respect to graphene (right).

The doping of the graphene by the Bi islands is limited to the area below the islands, resulting in an inhomogeneous doping concentration that shows a magnetotransport behavior which is expected for antidots. The scattering process at the islands seems to be phase breaking, thus suppressing the weak localization effect, and thereby impeding the assessment of the effect that the Bi islands have on the spin-orbit interaction in graphene.

Poster Contributions

Poster N	Name	Title
P.1	Phiw-Ondee Satjawoot	Structural study of reactive growth and interaction between cerium oxide and graphene on Ru(0001)
P.2	Pavel Procházka	ProLEED Studio: Simplifying Modeling of Low-Energy Electron Diffraction Patterns
P.3	Chris Schröder	SPA-LEED studies of the ordering of Au-induced Nanowires on Si(553)
P.4	Joachim Wollschläger	SPA-LEED studies on the epitaxy of ultra-thin Fe ₃ O ₄ films on SrTiO ₃ (001)
P.5	Niels Ganser	UHV-CVD on Ir(111) for the Growth of 2D Materials
P.6	Mohammad Tajik	Order-disorder phase transition on the dimerized Si(001) surface
P.7	Christian Kumpf	Boron Nitride on SiC(0001): A pathway towards unconventionally oriented single-layer graphene and twisted bilayer graphene
P.8	Markus Gruschwitz	Imaging Charge Densities at Interfaces with TEM
P.9	Peter Richter	Growth of crystalline CoCrFeNi high-entropy alloy thin films on LaAlO ₃ by magnetron sputtering
P.10	Niclas Tilgner	Intercalation of Graphene on SiC: New Materials and Emerging Physics
P.11	Lukas Schewe	Composition and band structure of aluminum alloyed-gallium oxide by XPS
P.12	Sergii Sologub	Intercalation of Pb using buffer layer on SiC(0001)

Structural study of reactive growth and interaction between cerium oxide and graphene on Ru(0001)

Satjawoot Phiw-Ondee¹, Linus Pleines¹, Jon-Olaf Kristponeit^{1,2}, Thomas Schmidt¹, Jens Falta^{1,2}

¹*Institute of Solid State Physics, University of Bremen, Otto-Hahn-Allee 1, 28359 Bremen, Germany*

²*MAPEX Center for Materials and Processes, P.O. Box 330 440, 28334 Bremen, Germany*

Cerium oxide (CeO_x) has catalytic properties to store oxygen by oxidation and release oxygen by reduction. Due to reduction, CeO_2 with the oxidation state Ce^{4+} shows the transition to Ce_2O_3 with the oxidation state Ce^{3+} by releasing its oxygen [1]. This transition is reversible.

Graphene (Gr) is known as hexagonal 2D-carbon material with sp_2 -hybridization [2]. Freestanding single-layer graphene shows a linear dispersion at Dirac point, where electrons behave massless [3]. Therefore, a freestanding single-layer graphene has a high electrical conductivity. An important interaction, which makes graphene freestanding, is the so-called intercalation. By exposing elements to a single-layer graphene on a substrate, these can be inserted under the graphene layer. For example, oxygen can be intercalated under graphene [4].

By combining cerium oxide with a single-layer graphene, it might be possible to combine the catalytic properties of CeO_x with the electrical properties of a single-layer graphene. This work deals with the study of interaction between cerium oxide and graphene on Ru(0001) by using a low-energy microscope (LEEM). The applied methods are micro low-energy electron diffraction (μLEED) and $\text{I}(\text{V})$ -LEEM. For the preparation of single-layer graphene on Ru(0001) in UHV, chemical vapor deposition (CVD) of ethylene and carbon segregation are used. A home-made evaporator is utilized for exposing cerium to Gr/Ru(0001) at different temperatures. The exposed cerium is oxidized with oxygen in the UHV. By exposing to cerium to graphene single-layer at high temperature 720°C , graphene is etched from CeO_x by releasing its oxygen to oxidize graphene. Two forms of cerium oxide in the area of graphene are observed by μLEED , $\text{CeO}_x(111)\text{R}8^\circ$ and CeO_x with the $(\sqrt{27} \times \sqrt{27})\text{R}30^\circ$ -superstructure.

References:

[1] T. Duchoň, F. Dvořák, M. Aulická, V. Stetsovych, M. Vorokhta, D. Mazur, K. Veltruská, T. Skála, J. Mysliveček, I. Matolínová and V. Matolín, *J. Phys. Chem. C*, 357-365, 118 (2014).

[2] P. Sutter and E. Sutter, *Advanced Functional Materials*, 2617-2634, 23 (2013).

[3] K. S. Novoselov, A. K. Geim, S. V. Morozov, D. Jiang, M. I. Katsnelson, I. V. Grigorieva, S. V. Dubonos and A. A. Firsov, *Nature*, 197–200, 438 (2005).

[4] P. Sutter, P. Albrecht, X. Tong, and E. Sutter, *J. Phys. Chem. C*, 6320-6324, 117 (2013).

ProLEED Studio: Simplifying Modeling of Low-Energy Electron Diffraction Patterns

Pavel Procházka¹, Jan Čechal^{1,2}

¹CEITEC – Central European Institute of Technology, Brno University of Technology, Purkyňova 123, 612 00 Brno, Czech Republic

²Institute of Physical Engineering, Brno University of Technology, Technická 2896/2, 616 69 Brno, Czech Republic

Low-energy electron diffraction (LEED) patterns hold precise information about the surface structure. However, extracting real space lattice periodicity from complex diffraction patterns can be challenging, mainly when dealing with superlattices that have large unit cells composed of multiple symmetry-equivalent domains, especially when these lack straightforward relationship to the substrate, such as patterns arising from molecular adsorbates. Fig. 1 illustrates a low-energy electron microscopy (LEEM) measurement and modeling of such a system.

In this contribution, we will introduce ProLEED Studio, a software tool designed to enable simple, precise, and intuitive modeling of experimental LEED patterns to determine 2D unit cells [1]. The interactive GUI facilitates real-time manipulation with any lattice points or diffraction spots, allows the loading of experimental patterns for direct comparison with the modeled diffraction patterns, and offers the ability to adjust the size of the modeled spots to reflect their varying intensities. Additionally, it provides functionality to pin real-space superstructure lattice points to the nearest substrate lattice point, aiding in identifying the closest commensurate lattice. Visualization tools for the unit cells, vectors, superlattice domains, and scale bars further simplify the modeling process, making ProLEED Studio not only a powerful tool but also an excellent educational resource.

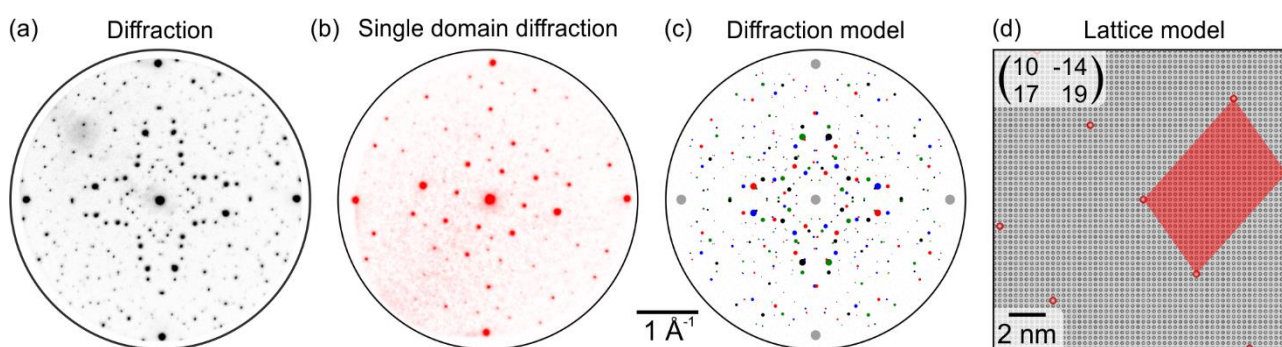


Fig 1. (a) Diffraction pattern of the Ag(001) substrate covered with a monolayer of 4,4'-biphenyl-dicarboxylic acid (BDA) arranged in a four-domain structure. (b) Diffraction pattern from a single superlattice domain. ProLEED Studio model of (c) reciprocal and (d) real-space lattice. The patterns were measured using low-energy electron microscopy (LEEM).

References

[1] P. Procházka, J. Čechal, *J. Appl. Cryst.*, 187, Vol. **57** (2024).

SPA-LEED studies of the ordering of Au-induced nanowires on Si(553)

C. Schroeder

University of Osnabrück, Department of Mathematics/Computer Science/Physics, Institute of Physics, BarbarasträÙe 7, 49069 Osnabrück, Germany

This research explores the formation and ordering of Au-induced nanowires on Si(553) surfaces using SPA-LEED. The Si(553) surface, characterized by its atomic steps, facilitates the formation of nanowires when covered with gold. The primary objective of this study is to determine the influence of coverage on the structural characteristics of these nanowires.

Through detailed SPA-LEED analysis, we examined the full width at half maximum (FWHM) and the position of diffraction spots to assess the quality and organization of the nanowires. Our findings indicate the substrate temperature during gold deposition significantly affects nanowire formation, influencing both the morphology and domain size. Additionally, we identified coverage-dependent phases, including the “Low Coverage Wire” and “High Coverage Wire” phases, each with unique structural properties, discovered by I. Song et al [1].

These results contribute to a deeper understanding of the optimal conditions for nanowire growth on Si(553) surfaces, providing valuable insights for future research and applications in nanotechnology.

[1] I. Song, ACS Nano, 10621, 9 (2015).

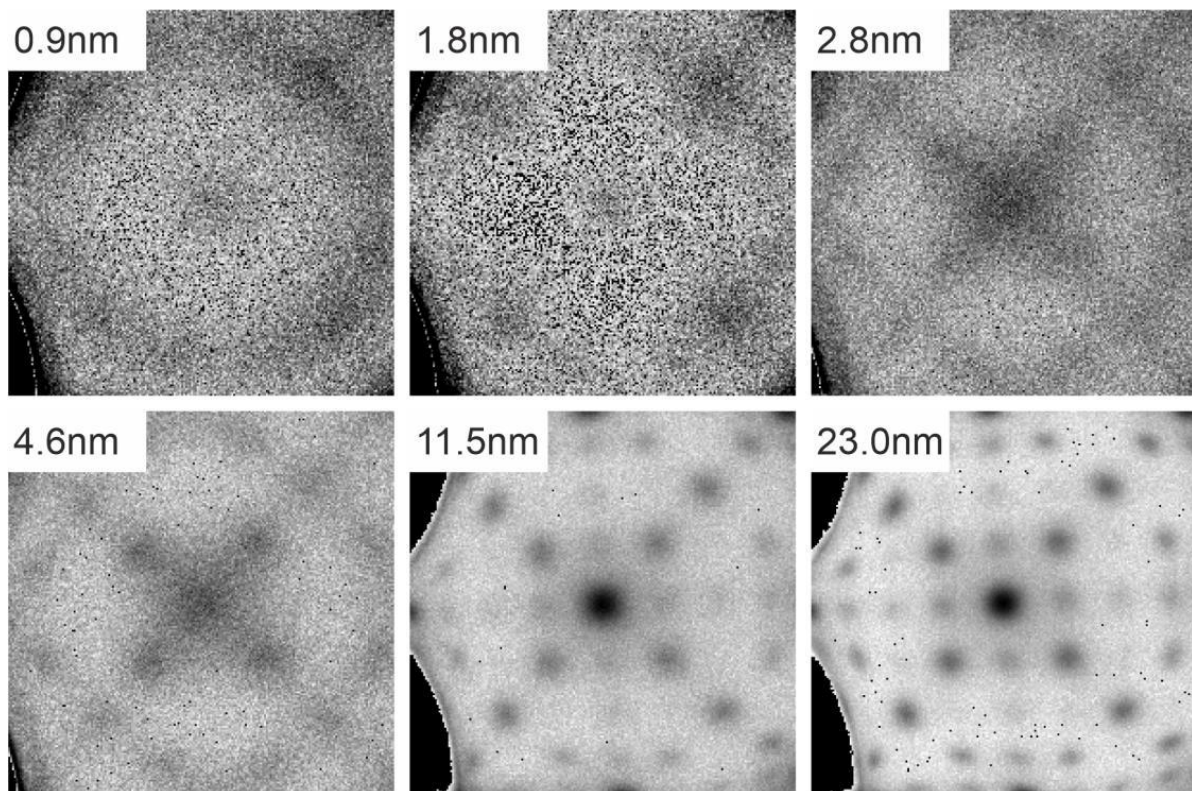
SPA-LEED studies on the epitaxy of ultra-thin Fe₃O₄ films on SrTiO₃(001)

A. Alexander, T. Kleideiter, T. Pollenske, K. Ruwisch, F. Bertram, J. Wollschläger

Institut für Physik, Universität Osnabrück, Germany

Ultrathin Fe₃O₄ films were grown step-by-step on SrTiO₃(001) substrates using reactive molecular beam epitaxy (Fe metal deposition in diluted O₂ atmosphere) at different growth temperatures. Surface sensitive spot profile analysis low energy electron diffraction (SPA-LEED) was used to characterise the surface morphology and structural information after each deposition step. After an initial growth phase for film thickness $t_f < 2.8$ nm, in which the films grow with apparent FeO rock salt structure, the films continue to grow with well-ordered Fe₃O₄(001) spinel structure.

Independent of the deposition temperature, defect density decreases with increasing film thickness, while crystallinity, i.e. structural quality, of the magnetite thin films increases with both increasing film thickness and increasing deposition temperature. The results show that mosaics and domains/grains can be found on the surface. Higher deposition temperatures do not cause any change in the mosaic spread angle but the mean domain size increases. Furthermore, for very low coverages ($t < 0.9$ nm) another growth-phase was found, which can be assigned to (111)-oriented Fe₃O₄ with hexagonal surface structure although deposited on a substrate with square surface structure.



Development of SPA-LEED pattern for Fe oxide films deposited on SrTiO₃(001) from hexagonal ($t_f = 0.9$ nm) via rocksalt ($t_f = 1.8$ - 2.8 nm) to spinel structure ($t_f < 4.6$ nm).

UHV-CVD on Ir(111) for the Growth of 2D Materials

N. Ganser¹, M. Kriegl¹, K. Omambac¹, M. Petrovic², C. Brand¹, S. Franzka³, B. Finke¹, T. Hartl⁴, T. Michely⁴, F.-J. Meyer zu Heringdorf^{1,3} and M. Horn-von Hoegen¹

¹Department of Physics and CENIDE, Universität Duisburg-Essen, D-47057 Duisburg, Germany

²Center of Excellence for Advanced Materials, Institute of Physics, Zagreb, Croatia

³Interdisciplinary Center for Analytics on the Nanoscale (ICAN), D-47057 Duisburg, Germany

⁴Institute of Physics II, Universität zu Köln, D-50937 Köln, Germany

Hexagonal boron nitride (*h*BN) is a 2D-Material with a wide band gap exhibiting the same crystal structure as graphene. It can be grown by scalable chemical vapor deposition (CVD) from a borazine $B_3N_3H_6$ precursor. Here we show that the *h*BN quality depends strongly not only on the growth temperature T_g but also on the dosing pressure p_{dose} .

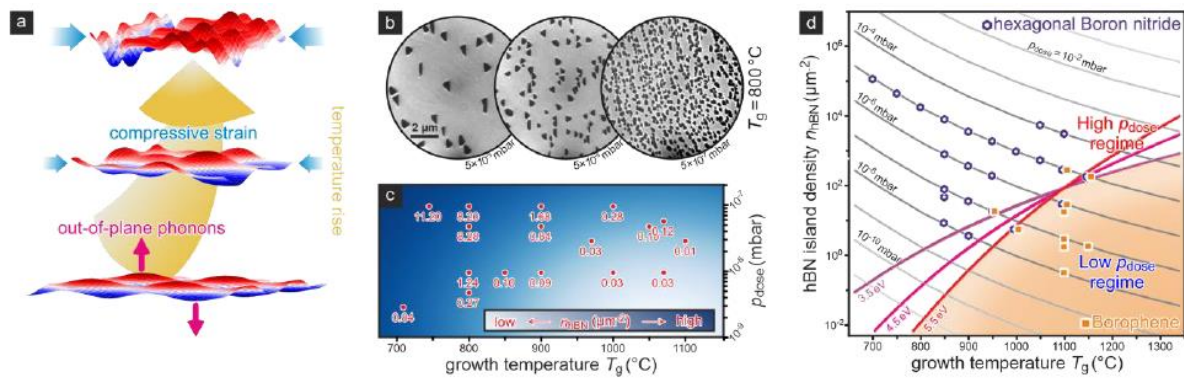


Figure 1: a) Illustration of Lifshitz membrane effect b) LEEM images showing n_{hBN} variation as function of p_{dose} . c) Plot of n_{hBN} as function of p_{dose} and T_g . d) phase diagram for T_g and p_{dose} .

A combined *in-situ* SPA-LEED and LEEM study on the defect and island density of *h*BN monolayers grown on Ir(111) at different T_g and p_{dose} reveals a negative thermal expansion coefficient of α_{hBN} , $900\text{ °C} = (-2.4 \pm 1.2) \times 10^{-6}\text{ K}^{-1}$. This value is consistent with theoretical predictions and caused by a non-linear dispersion relation for out-of-plane polarized transversal ZA phonon modes (Fig. 1a) as explained by the Lifshitz membrane effect [1]. Due to a strong interaction with the Iridium lattice the *h*BN layers grow epitaxially in the R0-phase and do not form wrinkles during the cooldown process [2]. However, their incommensurate registry to the Ir-lattice clearly indicates they grow independently of the underlying substrate.

Further measurements by SPA-LEED and LEEM (Fig. 1b) show a strong dependence of n_{hBN} on p_{dose} (mapped in Fig. 1c). We find that the quality of the *h*BN layers that can be achieved by increasing T_g is limited by the process of disintegration of the Borazine at $T_g > 950\text{ °C}$ resulting in growth of borophene instead [3], as depicted in the p_{dose} - T_g phase diagram shown in Fig. 1d [4]. Thus, it is possible to selectively grow either *h*BN or borophene from the same precursor [4].

[1] Lifshitz, I., Zh. Eksp. Teor. Fiz. **22**, 475 (1952)

[2] Petrović, M. et al., Appl. Surf. Sci. **420**, 504–510 (2017)

[3] Omambac, K. et al., ACS Nano **15**, 7421 (2021)

[4] Omambac, K. et al., ACS Nano **17**, 17946 (2023)

Order-disorder phase transition on the dimerized Si(001) surface

M. Tajik¹, C. Brand¹, A. Hucht^{1,2}, H. Mehdipour¹, G. Jnawali¹, J. D. Fortmann¹, R. Hild¹,
B. Sothmann^{1,2}, P. Kratzer^{1,2}, R. Schützhold^{3,4} and M. Horn-von Hoegen^{1,2}

¹Faculty of Physics, University of Duisburg-Essen, 47057 Duisburg, Germany

²Center for Nanointegration (CENIDE), University of Duisburg-Essen, 47057 Duisburg, Germany

³Institute of Theoretical Physics, Dresden University of Technology, 01062 Dresden, Germany

⁴Helmholtz-Zentrum Dresden-Rossendorf, 01328 Dresden, Germany

We investigate the critical behavior of the order-disorder phase transition of the buckled dimer structure of the Si(001) surface with spot profile analysis low-energy electron diffraction (SPALED) [1,2]. The continuous phase transition from the low-temperature $c(4\times 2)$ reconstruction to the high-temperature $p(2\times 1)$ reconstruction is monitored, showing the critical behavior near the transition temperature $T_C = 190$ K in agreement with the universality class of two-dimensional anisotropic Ising model as shown in Fig. 1. Also, density functional theory (DFT) is employed with three different functionals to calculate the coupling constants of effective lattice Hamiltonian describing the dimer interactions. The experimentally determined coupling constants, $J_{||} = -24.9$ meV and $J_{\perp} = -0.8$ meV, align with those obtained from DFT calculations.

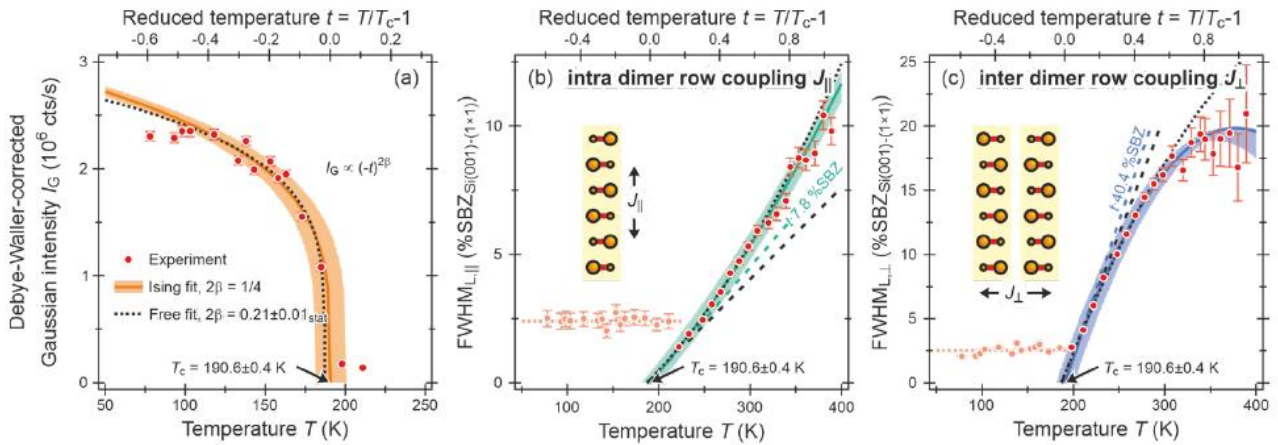


Figure 1. (a) Gaussian contributions to the $(3/4 - 1/2)$ spot intensity as function of temperature. (b,c) Temperature-dependent FWHMs of the Lorentzian contribution along and across the dimer rows corrected for the instrumental resolution, respectively.

[1] C. Brand et al., *Phys. Rev. Lett.* **130**, 126203 (2023).

[2] C. Brand et al., *Phys. Rev. B* **109**, 134104 (2024).

Boron Nitride on SiC(0001): A Pathway towards Unconventionally Oriented Single-Layer Graphene and Twisted Bilayer Graphene

Hao Yin^{1,2}, You-Ron Lin^{1,2}, Mark Hutter^{1,2}, Markus Franke^{1,2}, Shayan Parhizkar^{1,2}, Miriam Raths^{1,2}, Christian Wagner¹, Serguei Soubatch¹, F. Stefan Tautz^{1,2}, François C. Bocquet¹, Christian Kumpf^{1,2}

¹*Peter Grünberg Institut (PGI-3), Forschungszentrum Jülich, and Jülich Aachen Research Alliance (JARA), Fundamentals of Future Information Technology, 52425 Jülich, Germany*

²*Experimentalphysik IV A, RWTH Aachen University, 52074 Aachen, Germany*

In the field of van der Waals heterostructures, the twist angle between stacked two-dimensional layers is of utmost importance for the properties of the heterostructures. In this context, the growth of a single layer of unconventionally oriented epitaxial graphene was demonstrated, which forms in a borazine surfactant atmosphere [1]. The resulting graphene-R0° layer is aligned with the SiC lattice, and hence represents an important milestone towards high-quality twisted bilayer graphene. Here, we report on two preparation pathways utilizing the surfactant atmosphere: Boron nitride template layers formed on SiC(0001) at temperatures below 1100°C [2], and graphene-R0° mono-, as well as multilayers obtained at higher temperatures [3]. We report SPA-LEED and LEEM measurements, including an automatized LEEM-IV analysis for layer counting.

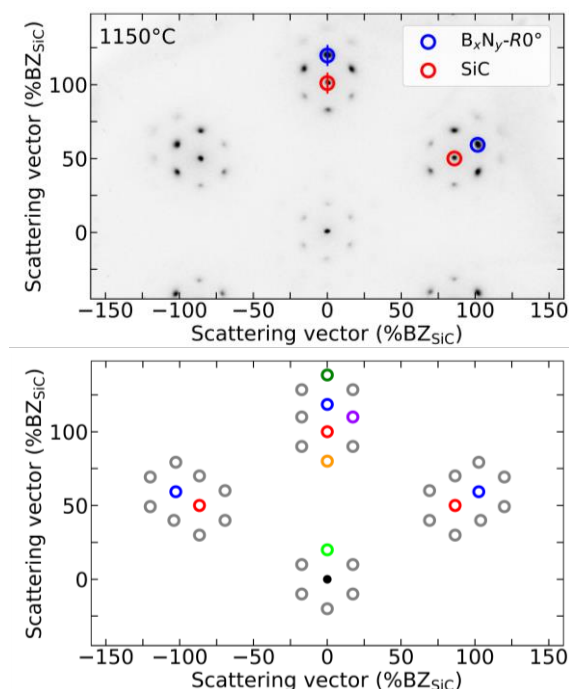


Fig. 1: SPA-LEED image and simulation of BN on SiC(0001) in R0°- orientation.

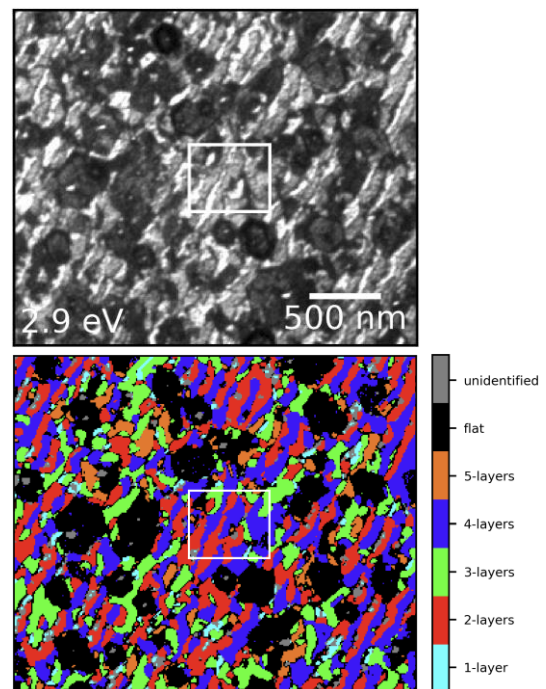


Fig. 2: BF-LEEM image and false colour representation of graphene multilayers.

- [1] F.C. Bocquet et al., Phys. Rev. Lett. **125**, 106102 (2020); H.-C. Shin et al., J. Am. Chem. Soc. **137**, 6897 (2015).
 [2] Y.-R. Lin et al., Phys. Rev. Mater. **6**, 064002 (2022).
 [3] H. Yin et al., Phys. Rev. Mater., under review.

Imaging Charge Densities at Interfaces with TEM

Markus Gruschwitz¹, Sergii Sologub^{1,2}, Steffen Schulze¹, Herbert Schletter¹, Christoph Tegenkamp¹

¹*Analytik an Festkörperoberflächen, TU Chemnitz, Reichenhainer Str. 70, 09126 Chemnitz*

²*Institute of Physics, NAS of Ukraine, Nauki avenue 46, 03028 Kyiv*

Differential phase contrast (DPC) is a long known contrast mechanism originated in the deflection of transmitted electrons heavily depending on the local electrical (or magnetic) fields in the sample [1]. By utilizing segmented detectors, the shift of the center of mass of the CBED pattern can be detected. Recent developments in conjunction with aberration corrected scanning transmission electron microscopes (STEM) demonstrated the ability to achieve atomically resolved DPC images [2]. The evaluation of such images allows an estimation of local charge densities.

The technique is applied to epitaxial monolayer graphene (MLG) on 6H-SiC(0001) (Fig. 1a) in comparison to Pb intercalated graphene. While the charge carrier mobility in MLG are limited by substrate-based charge transfer [3], Pb effectively decouples the former buffer layer and screens latter substrate influences resulting in almost perfectly charge neutral graphene [4]. Thus, imaging the local charge density is of great interest (Fig. 1c). In the buffer layer and graphene layer, defined spots of positive charges (carbon atomic cores) are surrounded by a delocalized cloud of π -electrons. By using the pristine substrate SiC to calibrate the charge densities, we approach the system quantitatively and discuss deviations due to screening effects and influences of the protective capping layer.

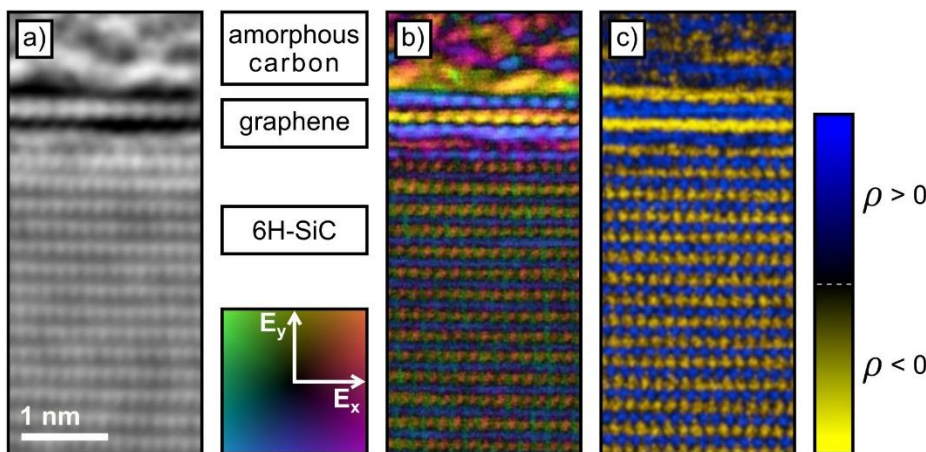


Fig. 1: (a) Integrated DPC-image. (b) Colour-coded visualisation of the vector. The wide range of 2D colour distribution necessary for this image makes a direct interpretation difficult. (c) Charge density derived from the DPC data. With only two colour gradients, the image yields an intuitive visualization of the charge density. [5]

[1] H. Rose, Ultramicroscopy, 251, Volume 2 (1976)

[2] N. Shibata, S. Findlay, Y. Kohno, H. Sawada, Y. Kondo, Y. Ikuhara, Nature Phys., 611, Volume 8 (2012)

[3] J. Ristein, S. Mammadov, T. Seyller, Phys. Rev. Lett., 246104, Volume 108 (2012)

[4] M. Gruschwitz, C. Ghosal, T.-H. Shen, S. Wolff, T. Seyller, C. Tegenkamp, Materials, 14, 7706 (2021)

[5] S. Schulze, M. Gruschwitz, H. Schletter, I. Alexandrou, M. Hietschold, C. Tegenkamp, Imaging & Microscopy, 34, 3/2020 (2020)

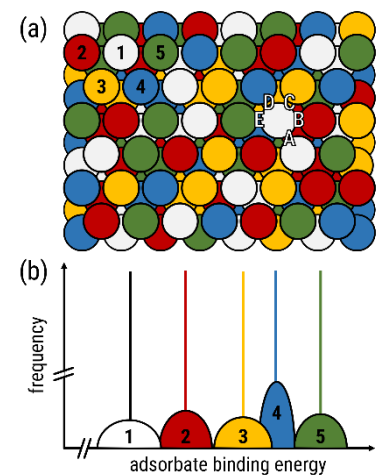
Growth of crystalline CoCrFeNi high-entropy alloy thin films on LaAlO₃ by magnetron sputtering

Peter Richter^{1,2}, Holger Schwarz^{1,2}, Thomas Seyller^{1,2}

¹*Technische Universität Chemnitz, Institut für Physik, Chemnitz, Deutschland*

²*Center for Materials, Architectures, and Integration of Nanomembranes (MAIN), Chemnitz, Deutschland*

Multicomponent alloys of at least four elements with near equimolar percentage were first reported and investigated by Cantor et al. [1] and Yeh et al. [2] in 2004 and are nowadays often referred to as High-Entropy Alloys (HEAs) [3]. This composition is expected to support the formation of single-phase solid solutions, which lead to extensive research on the mechanical properties of HEAs in the past decades, but surface physics are barely investigated so far. Recently, we have demonstrated the formation of crystalline thin films of CoCrFeNi via magnetron sputtering from homemade targets on MgO (100) single crystal substrates [4]. The single crystal character of the films and its epitaxial relation to the substrate were confirmed by X-ray diffraction (XRD) and transmission electron microscopy (TEM). Following a proper UHV surface treatment, the structural and electronic behaviour is accessible by means of low energy electron diffraction (LEED) and angle resolved photoelectron spectroscopy (ARPES).



In the present study, the proof of principle for this method of crystal fabrication is demonstrated by deposition of CoCrFeNi on LaAlO₃ (LAO) substrates. Access to surface studies on different CoCrFeNi crystal planes is achieved by the variation of the substrates surface orientation which determines the HEA growth direction. Since the lattice constants of LAO and CoCrFeNi are very similar, the occurrence of planar defects, which were observed more frequently on MgO, could be significantly reduced.

- [1] B. Cantor, I. T. H. Chang, P. Knight, et al., *Mater. Sci. Eng. A*, 213, 375-377, (2004)
- [2] J. W. Yeh, S. K. Chen, S. J. Lin, et al., *Adv. Eng. Mater.*, 299-303, 6, (2004)
- [3] D. B. Miracle and O. N. Senkov, *Acta Mater.* 122, 448 (2017)
- [4] H. Schwarz, J. Apell, H. K. Wong, et al., *Adv. Mater.* 35, 2301526 (2023).

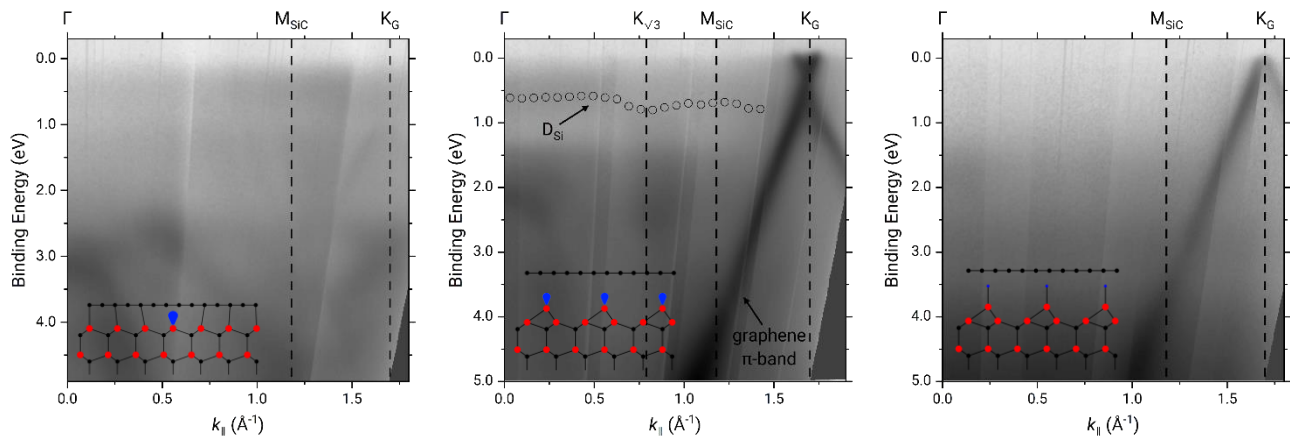
Intercalation of Graphene on SiC: New Materials and Emerging Physics

Niclas Tilgner^{1,2}, Susanne Wolff^{1,2}, Niels Rösch^{1,2}, Fabian Göhler^{1,2},
Philip Schädlich^{1,2}, Thomas Seyller^{1,2}

¹*Technische Universität Chemnitz, Institut für Physik, Chemnitz, Deutschland*

²*Center for Materials, Architectures, and Integration of Nanomembranes (MAIN),
Chemnitz, Deutschland*

The synthesis of new graphene-based quantum materials by intercalation is an auspicious approach. Here, the interface of graphene and silicon carbide provides a platform to, on the one hand, stabilize new materials, while the decoupled graphene acts as a protective layer. On the other hand, proximity effects between graphene and the intercalant provide the basis for emerging new physics. We present recent developments from our group covering a wide range of intercalant species, including chalcogens [1], bismuth, and experiments concerning sequential multi-element intercalation. Special focus will be placed on Mott-Hubbard Metal-Insulator transitions accessible via silicon intercalation [2].



[1] S. Wolff, N. Tilgner, F. Speck, et al., *Adv. Mater. Interfaces*, 11, 2300725 (2024)

[2] N. Tilgner, P. Schädlich, F. Göhler, et al., *manuscript in preparation*.

Composition and band structure of aluminum alloyed-gallium oxide by XPS

L. Schewe^{1*}, J. Rehm², M. C. Kao³, V. Vonk³, Z. Galazka², S. B. Anooz², A. Popp²,

and J. I. Flege¹

¹*Fachgebiet Angewandte Physik und Halbleiterspektroskopie, Brandenburgische Technische Universität Cottbus-Senftenberg, Cottbus, Brandenburg, Germany*

²*Leibniz-Institut für Kristallzüchtung, Berlin, Germany*

³*CXNS-Center for X-Ray and Nano Science, Deutsches Elektronen-Synchrotron, Hamburg, Germany*

Beta-phase gallium oxide is a transparent, wide-gap semiconductor with a band gap of 4.85eV [1] and promising prospects for applications in high-power devices. Considering its higher calculated breakdown field [2], β -gallium oxide is predicted to outperform well established materials such as silicon carbide and gallium nitride for high-power switching. To further increase the high-power capabilities, as suggested by the Baliga figure of merit, $BFOM = \epsilon\mu E_b^3$ [3], it is required to increase the electron mobility μ and electric breakdown field E_b . The electron mobility is highly dependent on the material's crystallinity and lack of defects, thus highly dependent on the growth technique. Moreover, the electric breakdown field can be increased by alloying the oxide with aluminum.

The present work discusses structural and electronic properties of $\beta - (Al_xGa_{1-x})_2O_3$ thin films grown by metal organic vapour-phase epitaxy and bulk crystals grown by the czochralski method. The achieved Al content ranges up to 30%. The Al concentration has been measured by X-ray photoelectron spectroscopy (XPS) and will be compared to the Al content calculated from the lattice parameter measured by X-ray diffraction (XRD) for thin films and inductively coupled plasma optical emission spectrometry (ICP-OES) for bulk samples. Additionally, the thin films have been investigated through XPS depth profiling obtained by sequential Argon ion sputtering, revealing lower aluminum content at the sample surface, indicating possible surface segregation of gallium. Additionally, the samples were cross checked with reference gallium oxide and aluminum oxide samples to confirm stoichiometric composition of the grown samples. Furthermore, the band gap has been determined by electron loss spectra from XPS and optical absorbance measurements. The obtained band gap to Al relation will be compared to the Al content measured with XPS, XRD and ICP-OES for corresponding samples.

[1] H.H. Tappin, Phys. Rev., 140, A316 (1965).

[2] M. Higashiwaki, et al., Appl. Phys. Lett., 100, 013504 (2012)

[3] B.J. Baliga, J. Appl. Phys., 1759-1764, 53 (1982)

[4] Z. Galazka, et al., J. Appl. Phys. 133, 035702 (2023)

Intercalation of Pb using buffer layer on SiC(0001)

Sergii Sologub^{1,2}, Markus Gruschwitz², and Christoph Tegenkamp²

¹*Institute of Physics, NAS of Ukraine, Nauki avenue 46, 03028 Kyiv*

²*Institut für Physik, TU Chemnitz, Reichenhainer Str. 70, 09126 Chemnitz*

Charge neutrality [1] as well as potential superconductivity [2] and induced SOC of epitaxial graphene by Pb intercalation recently sprouted great interest. We investigated the peculiarities of the intercalation of Pb using buffer layer on 4H/SiC(0001) and 6H/SiC(0001) by SPA-LEED, SEM and STM techniques. Although proposed as an energetically unfavorable process [3], we optimize the intercalation by varying the coverage of deposited Pb, annealing temperature and duration, as well as numbers of deposition-annealing cycles. In particular, repeated cycles of 10-20 ML Pb-deposition at RT followed by annealing to 500 °C for 5 min were effective for the formation of the stripe intercalation phase, especially with additional annealing to 700 °C in every two cycles. The latter annealing usually resulted in the full deintercalation but it speeded up and improved the efficiency of the next intercalation cycles.

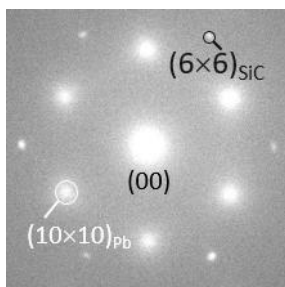


Fig. 1

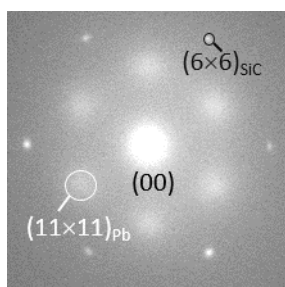


Fig. 2

On the other hand, the long-term annealing (more than 15 hours at 330-350 °C) of the 20-40 ML Pb coverage deposited on the stripe-phase substrate resulted in transformation of the later into the bubble one which was accompanied by corresponding changes in STM images and LEED patterns. In particular, (10×10) LEED spots associated with the stripe phase formation (Fig. 1) are shifted in the $\sim(11\times 11)$ positions attributed to the bubble phase (Fig. 2). Even more interesting that this transformation was *reversible*, i.e., a 5 min.-500 °C-annealing of the bubble phase restored the (10×10) spot position and the stripe phase.

Furthermore, using the samples with “undergrown” buffer layer was shown to facilitate and speed up the Pb intercalation. In addition, the orientation of SiC terraces perpendicularly to the long edges of rectangular samples seems to be helpful for improving the intercalation process. Also of importance is that residual Pb clusters remaining on the surface after the intercalation processes can be mainly removed by annealing to 400 °C.

[1] Philip Schädlich *et al.*, Adv. Mater. Interfaces, 2300471, 10 (2023).

[2] Tong Zhang *et al.*, Nat. Phys., 104, 6 (2010).

[3] Yong Han *et al.*, Carbon, 336, 205 (2023).

[4] Yong Han, *et al.*, J. Phys. Chem. Lett., 7053, 14 (2023).